Positron Studies of Defects 2011

Thermal stability of Mg$_y$Ti$_{1-y}$ thin films investigated by positron annihilation spectroscopy

A. Anastasopol[1*], S.W.H. Eijt[1], H. Schut[1], F.M. Mulder[1], F. Plazaola[2], B. Dam[3]

[1]*Department of Radiation, Radionuclides & Reactors, Faculty of Applied Sciences, Delft University of Technology, Mekelweg 15, NL-2629 JB Delft, The Netherlands*
[2]*Elektrizitate eta Elektronika Saila, Euskal Herriko Unibertsitatea, p.k. 644, 48080 , Bilbao, Spain*
[3]*Department of Chemical Engineering, Faculty of Applied Sciences, Delft University of Technology, Julianalaan 136, NL- 2628 BL Delft, The Netherlands*

Abstract

   Mg-Ti compounds are attractive candidates as hydrogen storage materials for their fast sorption kinetics and high storage capacity. In this context, an investigation of their thermal stability is of great importance. The thermal stability of Mg$_y$Ti$_{1-y}$ thin films was investigated using positron annihilation spectroscopy. Despite the positive enthalpy of mixing of Mg and Ti, positron Doppler Broadening of Annihilation Radiation (DBAR) depth profiling showed that Mg$_{0.9}$Ti$_{0.1}$ films are stable up to 300°C. However, for Mg$_{0.7}$Ti$_{0.3}$ films, segregation of Mg and Ti was observed at 300°C by the appearance of a clear Ti signature in the S-W diagrams and in the Doppler broadening depth profiles analyzed using VEPFIT. The thickness of the 250-300 nm thin films remained unchanged during the heating treatments. We further present ab-initio calculations of positron lifetimes of the corresponding metal and metal hydride phases for comparison to our previous positron annihilation lifetime spectroscopy (PALS) study.

1. Introduction

   Magnesium hydride is an attractive material for hydrogen storage because of its light weight and wide availability. However, the hydrogen sorption reactions have very slow kinetics and the enthalpy of formation is rather high. In combination with Ti, the sorption kinetics is greatly improved [1] for Ti-fractions larger than ~15%. Notten and co-workers [1-3] reported the synthesis of Mg-Ti alloys via electron beam deposition. An interesting aspect is that in thermodynamic equilibrium, Mg and Ti are immiscible. Several studies have reported the synthesis of Mg-Ti alloys through other non-equilibrium synthesis techniques, both as thin films [3-5] and as powders [6].

---
* Corresponding author. Tel.: +31-15-278 3656; fax.: +31-15-278 6422.
E-mail: a.middelkoop-anastasopol@tudelft.nl

Although the structure of the Mg-Ti films shows long-range coherence in X-ray diffraction, Baldi *et al*. [7] showed that a certain level of chemical segregation between Mg and Ti occurs, with domain sizes in the nanometer scale. This is also supported by the positron Doppler broadening study on Mg_yTi_{1-y} thin films by Leegwater *et al*. [8]. It could thus be expected that when such an alloy is submitted to heat treatments, the segregation of Mg and Ti will become more pronounced. Here we present a positron annihilation spectroscopy (PAS) study on the – surprisingly high – thermal stability of the Mg_yTi_{1-y} thin films, in which we analyze two compositions, namely $Mg_{0.9}Ti_{0.1}$ and $Mg_{0.7}Ti_{0.3}$. Further, we compare positron lifetimes calculated from first-principles with the experimental positron lifetimes extracted from our previous positron annihilation lifetime spectroscopy (PALS) measurements on TiH_x, $Mg_{1-y}Ti_yH_x$ and $Mg_{1-y}Ti_y$ films [8, 9], which indicated saturation trapping in di-vacancies.

2. Experimental

$Mg_{0.7}Ti_{0.3}$ and $Mg_{0.9}Ti_{0.1}$ thin films were deposited on suprasil substrates by DC magnetron co-sputtering of Mg and Ti under ultra high vacuum at room temperature. A Pd capping layer with a thickness of 1-2nm was added to prevent oxidation of Mg. Subsequently, the films were loaded with H_2 at room temperature for 24 hours, under a pressure of 0.1bar. The hydrogenated $Mg_{0.7}Ti_{0.3}H_x$ films were heated to 300 ^{o}C, where hydrogen desorption occurs in 7-8 hours as monitored by X-ray diffraction (XRD). Both XRD and Doppler Broadening of Annihilation Radiation (DBAR) depth profiling indicated the return to the initial metallic state. Subsequently, the films were heated to a temperature of 200°C, 250°C or 300°C for 40 hours under a vacuum of 10^{-3} mbar. The $Mg_{0.9}Ti_{0.1}H_x$ films were desorbed during the first part of the heating run at 250°C or 300°C. After each heating treatment, the DBAR profiles of the films were measured with positron implantation energies ranging from 0.1-25keV. The Doppler broadening S and W annihilation parameters were extracted in the same manner as described in Ref. [10]. The S parameter represents the annihilation of positrons with low momentum valence electrons. This parameter is especially sensitive to the presence of vacancies. The W parameter corresponds to the annihilation with high momentum core electrons, and is sensitive to the local chemical surrounding of the annihilation site. The data were fitted using VEPFIT [11].

Ab-initio calculations of the positron lifetimes based on density functional theory (DFT) were performed using the AT-SUP method [12], employing the following two approaches for the correlation energy and enhancement: (1) the local density approximation (LDA) with the Boronski-Nieminen (BN) approach to the correlation energy, (2) the generalized gradient approximation (GGA) (see Ref. [13] for details of the applied calculational methods). These two approaches yielded only small differences in the positron lifetimes, therefore the averaged values are presented here. The positron lifetimes for rutile and fluorite MgH_2 were calculated as a function of lattice parameter valid in the range for $Mg_{1-y}Ti_yH_x$ films (see Ref. [14]) in order to facilitate a comparison with the experimental lifetimes.

3. Results and Discussion

3.1 Doppler broadening depth profiling study of the thermal stability of Mg_yTi_{1-y} thin films

Positron annihilation depth profiles were obtained on Mg_yTi_{1-y} thin films by varying the positron implantation energy. The higher the kinetic energy of positrons in the positron beam, the deeper they penetrate into the material. Figure 1 represents the S parameter (Figure 1a) and W parameter (Figure 1b) depth profiles for the $Mg_{0.9}Ti_{0.1}$ films. VEPFIT analysis showed that the thickness of the films was about 300nm, which did not change as a result of the heating treatment. The presence of the film after each heat treatment and its thickness of about 300nm was also confirmed by scanning electron microscopy, showing that evaporation was negligible. The presence of three layers was assumed in the VEPFIT analysis: 1) a very thin Pd layer at the surface, 2) a $Mg_{0.9}Ti_{0.1}$ layer underneath and 3) the suprasil substrate. The obtained best-fit parameters are represented by the corresponding depth profiles (solid lines) in the figures, which are in a good agreement with the measured data. As indicated in the figure, positrons with energies below 10keV annihilate primarily within the $Mg_{0.9}Ti_{0.1}$ layer. At higher energies, positrons increasingly annihilate in the suprasil substrate. The S parameter characteristic for the $Mg_{0.9}Ti_{0.1}$ layer was fitted to 0.644 and the W parameter was found to be 0.245. These values remained unchanged after each heating treatment.

In a similar experiment, $Mg_{0.7}Ti_{0.3}$ films were also annealed at temperatures ranging from 200°C to 300°C. The corresponding positron depth profiles are plotted in figure 2. The VEPFIT analysis was performed using the same model as for the $Mg_{0.9}Ti_{0.1}$ samples. The fits are in a very good agreement to the measured data. The thickness of the films obtained from the VEPFIT analysis was ~250nm and remained essentially unchanged after the heating

treatments. The S parameter (figure 2a) for the $Mg_{0.7}Ti_{0.3}$ layer of the sample annealed at $200^{o}C$ was measured to be 0.643. This value is close to $Mg_{0.7}Ti_{0.3}$ reference samples that were not subjected to heat treatment. The film annealed at $250^{o}C$ presents a slightly lower S value of 0.640. However, after the $300^{o}C$ heat treatment, the S parameter of $Mg_{0.7}Ti_{0.3}$ was seen to decrease strongly to a value of 0.625.
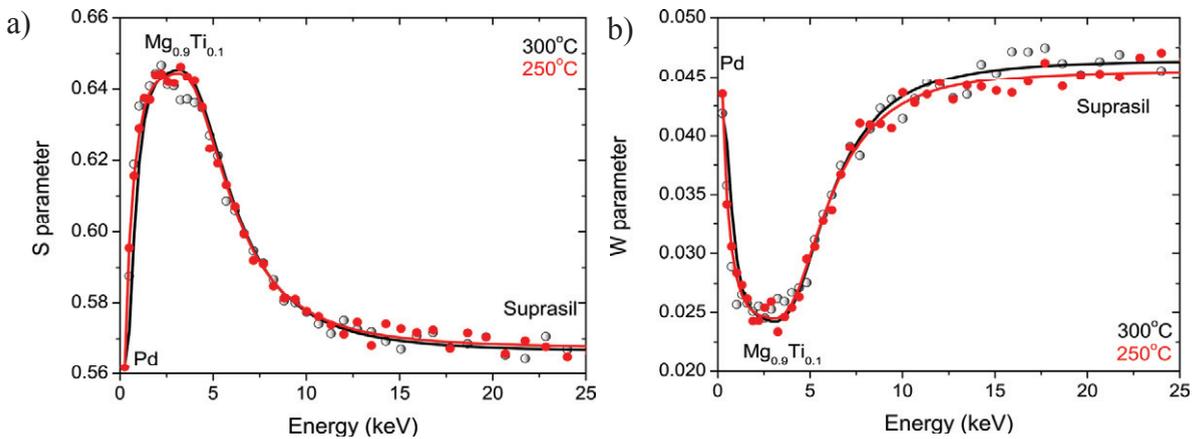
Figure 1. Positron depth profiles of $Mg_{0.9}Ti_{0.1}$ metallic films after heating treatments at $250^{o}C$ (full circles) and $300^{o}C$ (open circles). The continuous line represents the best-fits to the data using VEPFIT analysis. a) The evolution of the S parameter as a function of positron energy; b) The evolution of the W parameter as a function of positron energy.
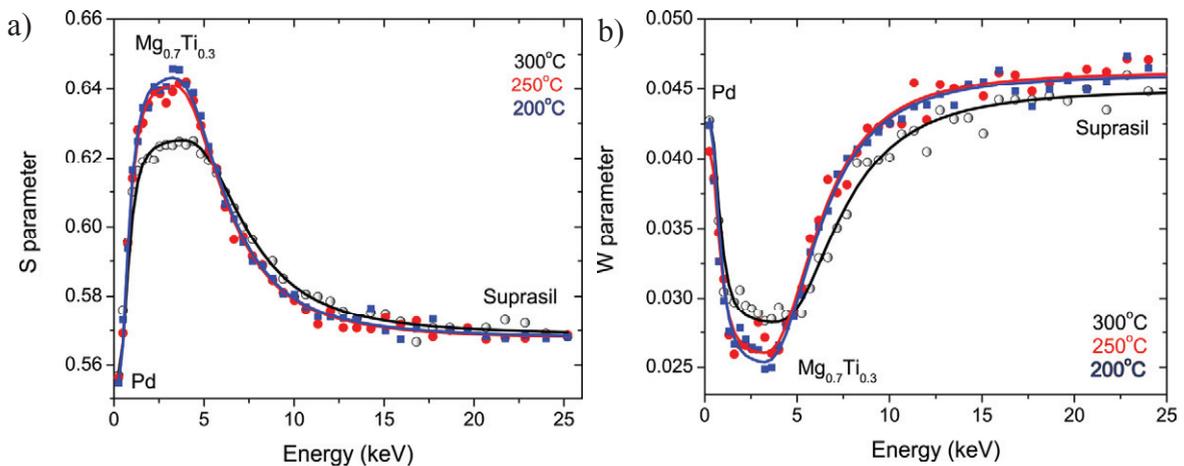
Figure 2. Positron depth profiles of $Mg_{0.7}Ti_{0.3}$ metallic films after heating treatments at $200^{o}C$ (stars), $250^{o}C$ (full circles) and $300^{o}C$ (open circles). The continuous line represents the best-fits to the data using VEPFIT analysis. a) The evolution of the S parameter as a function of positron energy; b) The evolution of the W parameter as a function of positron energy.

The W parameter of the $Mg_{0.7}Ti_{0.3}$ layer shows an opposite trend, as it increases with increasing annealing temperature. The increase in W parameter is more pronounced than the decrease in the S parameter. For the sample annealed at $200^{o}C$ and $250^{o}C$, the W parameter remains rather close to the reference value of 0.025. After the annealing at $300^{o}C$, however, the W parameter is strongly increased by 10%. This is indicative of important changes in the local chemical surroundings of the annihilation site, as the W parameter is characteristic of the annihilation with (semi-)core electrons, and points to increased annihilation with Ti atoms.

This effect is clearly discerned in S-W diagrams. Clement *et al*. [15] showed that presenting the positron annihilation data in a S-W diagram is a very useful approach, due to the linear relation between the S and W parameters. In figure 3, the S-W diagrams for the $Mg_{0.7}Ti_{0.3}$ (figure 3a) and $Mg_{0.9}Ti_{0.1}$ (figure 3b) samples are plotted. The experimental S-W curves run counter clockwise with increasing positron implantation energy, corresponding to increasing average depths below the surface of the sample. At very low positron energies, the annihilation parameters are characteristic for the Pd capping layer. At intermediate energies, positrons are implanted

primarily in the Mg_yTi_{1-y} film where they get trapped and annihilate in defects of the Mg_yTi_{1-y} film. Positrons with energies higher than 10 keV annihilate mostly in the suprasil substrate. Both for the $Mg_{0.9}Ti_{0.1}$ and $Mg_{0.7}Ti_{0.3}$ films, the S and W parameters are very close to those for a pure Mg layer, despite the increased Ti-fractions. This is caused by the higher affinity of positrons for Mg rather than for Ti [16], with a difference in positron affinity A_+ of $\Delta A_+ \cong 2.1\ eV$ [16]. The annihilation of the positron therefore will contain, almost exclusively, information about the Mg areas in the layer, even when these areas are intrinsically intermixed with Ti domains on nanometer length scales. Positron trapping in Mg domains, namely, will already occur for domain sizes as small as ~0.8 nm, as can be estimated from a spherical well potential with a depth $\Delta A_+ = 2.1$ eV according to: $d_{min} > \dfrac{\pi\hbar}{\sqrt{2m_o\Delta A_+}}$ [17]. The annihilation parameters of annealed Mg are therefore taken as the S-W reference point in the S-W plot of figure 3. The solid lines represent the results of the VEPFIT analysis. The fits lead to a straight line from the surface to the Mg_yTi_{1-y} layer and second straight line to the substrate. The two lines both closely match the data for each sample, showing the validity of the layered model with a single Pd-capped Mg_yTi_{1-y} layer on top of the suprasil substrate.
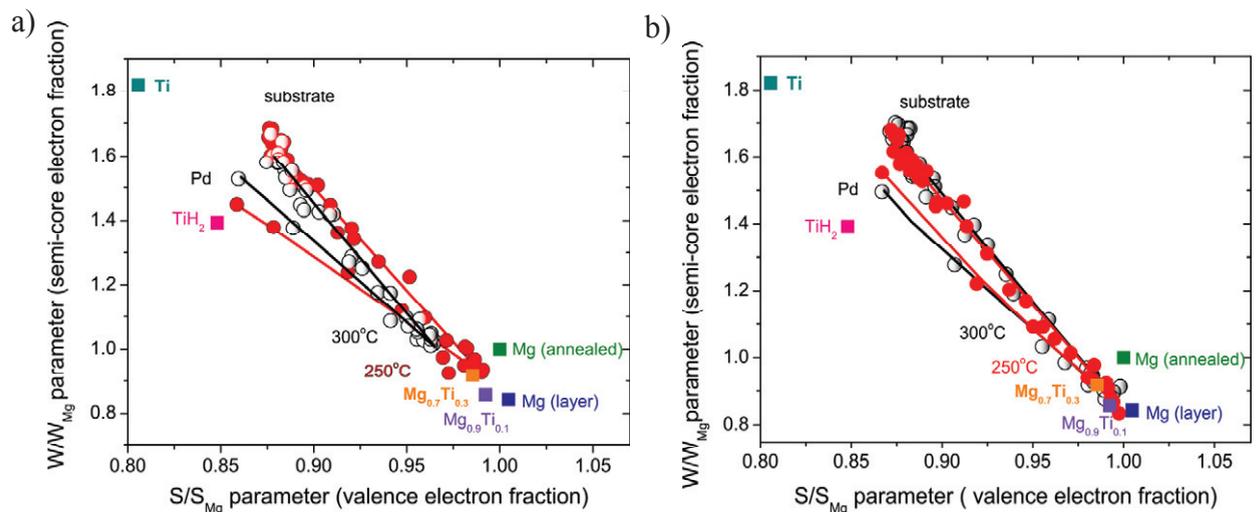
Figure 3. S-W plots of (a) $Mg_{0.7}Ti_{0.3}$ and (b) $Mg_{0.9}Ti_{0.1}$ metallic films. The full lines represent the VEPFIT analysis.

The S-W diagram for the $Mg_{0.7}Ti_{0.3}$ films shows a clear shift towards higher W and lower S parameter value after the final 300 °C heat treatment, pointing to increased annihilation with Ti atoms as the S-W point has moved significantly in the direction of the S-W points of a TiH_2 film and of an annealed Ti bulk sample (figure 3a). This implies that clusters of Ti (or TiH_2) exist in the $Mg_{0.7}Ti_{0.3}$ films which are substantially larger than for the as-deposited or hydrogenated films. Large Ti clusters with significant vacancy concentrations could still act as a positron trap for positrons implanted in the cluster, despite of the higher positron affinity for Mg. The formation of Ti based precipitates in the films essentially points to a considerable segregation of Ti and Mg within the films, and can indeed be expected since Mg and Ti have a positive enthalpy of mixing. An alternative explanation, however, could be that the increased detection of Ti atoms may also result from the creation of defects at the interfaces [18] during this final heat treatment, leading to trapping of positrons at the interface of Mg areas with Ti or TiH_2 clusters.

In the S-W diagram of $Mg_{0.9}Ti_{0.1}$, it is very clear that in this case no visible change occurs in either S or W parameters during heat treatments, even after the final heat treatment at 300 °C. This somewhat surprising result, which contrasts with the behaviour of $Mg_{0.7}Ti_{0.3}$, seems to indicate that the lower Ti composition in the $Mg_{0.9}Ti_{0.1}$ film does not permit the formation of large enough clusters of Ti (or TiH_2) that will act as preferential trapping sites. Also, it could point to a higher stability of the coherent Mg-Ti alloy (with only a chemical segregation on nanoscale dimensions) against heating treatments at low Ti fractions. Further positron annihilation and in-situ X-ray diffraction studies expectedly will shed light on the intriguing evolution of the nanostructure of $Mg_{1-y}Ti_y$ and $Mg_{1-y}Ti_yH_x$ films.

3.2 Positron lifetime of rutile and fluorite MgH₂ and fluorite TiH₂ metal hydrides

In figure 4, we present the theoretical positron lifetimes of rutile and fluorite MgH_2 and fluorite TiH_2, calculated using the experimental lattice parameters deduced for hydrogen loaded $Mg_{0.9}Ti_{0.1}H_x$, $Mg_{0.7}Ti_{0.3}H_x$ and TiH_x films, respectively. Saturation trapping was observed for all metal and metal hydride films [8]. Qualitatively, these calculated positron lifetimes for the defect-free metal hydrides seem to follow closely the empirical dependence $\tau[ps] = 7.2\ V[Å^3]$ on volume per formula unit, despite differences in their electronic structure – TiH_2 is a metal, whereas both rutile and fluorite MgH_2 are insulators – and crystal structure. The calculated positron lifetime for rutile MgH_2 is close to the value of 219.5 ps recently reported by Luna *et al.* [19], while the calculated positron lifetime for TiH_2 is slightly smaller than the value of 152 ps reported by Kulkova *et al.* [20]. The calculated positron lifetime for defect-free Mg is close to previously reported theoretical and experimental values, and is much higher than those of the $Mg_{1-y}Ti_yH_2$ systems. This is expected, since the two additional hydrogen atoms per formula unit present in the latter case will lead to a strong increase in local electron density at the (interstitial) positron annihilation site. The volume dependence of the positron lifetime observed for the metallic $Mg_{1-y}Ti_y$ films is well-understood, and scales proportional to the volume per metal atom (Figure 4), as expected for the di-vacancy [21]. The Mg-Ti lattice contracts proportionally to the Ti-fraction [7], reducing the size of the di-vacancy. This leads to a larger electron density present at the positron trapping site with correspondingly higher positron annihilation rates. The experimental value of (312±4) ps for Mg films fits the calculated value of 316 ps for the Mg di-vacancy.
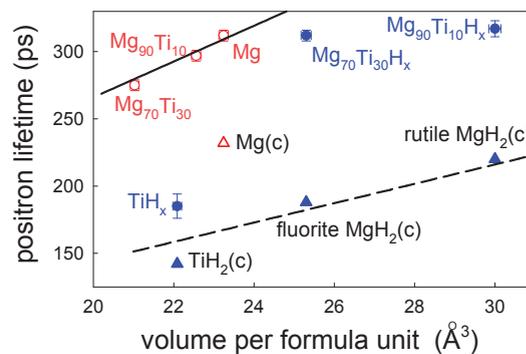
Figure 4. Calculated positron lifetimes for defect-free Mg, MgH₂ and TiH₂ (indicated by "(c)") compared with experimental positron lifetimes [8] of $Mg_{1-y}Ti_y$, $Mg_{1-y}Ti_yH_x$ (y=0.1, 0.3) and TiH_x thin films. The dashed line following $\tau[ps] = 7.2\ V[Å^3]$ is shown for a comparison with the ab-initio results; the solid line is a fit according to $\tau[ps] = 13.3\ V[Å^3]$ for the Mg di-vacancy.

The positron lifetime of the TiH_x film indicates that, in contrast to the $Mg_{1-y}Ti_y$ and $Mg_{1-y}Ti_yH_x$ (y=0.1, 0.3) films, the vacancy-related defect most likely correspond to a Ti mono-vacancy. The experimental positron lifetimes for the $Mg_{1-y}Ti_yH_x$ (y=0.1, 0.3) films show relatively large shifts relative to the calculated values for defect-free MgH_2. This indicates that lattice relaxation around the V_{Mg}-V_{Mg} (or V_{Mg}-V_H) di-vacancies is significant. Also, the presence of larger open volume defects involving the presence of more hydrogen vacancies seems possible. Recent neutron diffraction results, namely, showed indeed that abundant hydrogen vacancies can be present in Mg/Ti based metal hydrides. In nanostructured ball-milled MgH_2-TiF_3 powders, very high hydrogen vacancy concentrations of up to ~10% were found [22], induced by size effects and local strain due to the presence of many interfaces, including those between the MgH_2 and TiH_2 domains. We therefore recently started an ab-initio study of the positron lifetimes of small vacancy clusters in both fluorite and rutile MgH_2 which will be reported in a subsequent article. In contrast to the observed decrease in positron lifetime according to $\tau = \alpha V$ seen for the di-vacancy in the $Mg_{1-y}Ti_y$ films and for the calculated lifetimes for the defect-free metal hydrides, the experimental positron lifetime for the $Mg_{1-y}Ti_yH_x$ films does not follow this trend. The positron lifetime τ of the fluorite $Mg_{0.7}Ti_{0.3}H_x$ film is almost the same as for the rutile $Mg_{0.9}Ti_{0.1}H_x$ film, despite the large difference in volume per formula unit V. This indicates that more local open volume is present, which may induce a larger mobility of H (and Mg) in the fluorite MgH_2 system, aiding to the much faster hydrogen kinetics seen in fluorite phase MgH_2 relative to rutile phase MgH_2. We expect that our ab-initio study in progress of the positron lifetimes of small vacancy clusters in both fluorite and rutile MgH_2 may provide valuable insights in the fast hydrogen kinetics of the fluorite phase $Mg_{1-y}Ti_yH_x$ films.

4. Conclusion

In conclusion, positron Doppler broadening measurements on coherent Mg_yTi_{1-y} films can be used to measure the effects of thermal treatments on the nanoscale mixture of Mg and Ti. The samples that contained a higher amount of Ti ($Mg_{0.7}Ti_{0.3}$) show a clear signature of Ti as the W parameter increased significantly after the final heat treatment at 300°C, indicating that a pronounced segregation between Mg and Ti occurs. Surprisingly, the Doppler depth-profiles of the films that contained a lower amount of Ti ($Mg_{0.9}Ti_{0.1}$) maintained the same positron annihilation profile as the reference samples throughout the same set of heating treatments. This result can be explained by the low amount of Ti that did not permit the formation of large enough Ti precipitates. The calculated positron lifetimes for defect-free MgH_2 and TiH_2 are significantly lower than that of Mg, caused by the presence of the hydrogen atoms, leading to higher electron densities at the (interstitial) positron annihilation sites. The experimental positron lifetimes of $Mg_yTi_{1-y}H_x$ films, in contrast, are high, indicating either the occurrence of large local lattice relaxations around Mg-Mg (or Mg-H) di-vacancies or the presence of larger vacancy-related defects. The presence of vacancies seems important to understand the fast hydrogen sorption kinetics of fluorite MgH_2.

References

[1] P. Vermeulen, R.A.H. Niessen, and P.H.L. Notten, Electrochem. Comm. 8 (2006) 27-32.
[2] R.A.H. Niessen and P.H.L. Notten, Electrochem. Solid-State Lett. 8 (2005) A534-A538.
[3] P. Vermeulen, R.A.H. Niessen, D.M. Borsa, B. Dam, R. Griessen, and P.H.L. Notten, Electrochem. Solid-State Lett. 9 (2006) A520-A523.
[4] T. Mitchell, S. Displas, P. Tsakiropoulos, J.F. Watts, and J.A.D. Matthew, Phil. Mag. A 82 (2002) 841-855.
[5] D.M. Borsa, R. Gremaud, A. Baldi, H. Schreuders, B. Dam, R. Griessen, P. Vermeulen, and P.H.L. Notten, Appl. Phys. Lett. 88 (2006) 241910.
[6] G. Liang and R. Schulz, J. Mater. Sci. 38 (2003) 1179-1184.
[7] A. Baldi, R. Gremaud, D.M. Borsa, C.P. Baldé, A.M.J. van der Eerden, G. L. Kruijtzer, P.E. de Jongh, B. Dam and R. Griessen, Int. J. Hydrogen Energy 34 (1999) 1450-1457.
[8] H. Leegwater, H. Schut, W. Egger, A. Baldi, B. Dam, and S.W.H. Eijt, Appl. Phys. Lett. 96 (2010) 121902.
[9] S.W.H. Eijt, H. Leegwater, H. Schut, A. Anastasopol, W. Egger, L. Ravelli, C. Hugenschmidt, and B. Dam, J. Alloys Compd. 509S (2011) S567-S571.
[10] S.W.H. Eijt, R. Kind, S. Singh, H. Schut, W.J. Legerstee, R.W.A. Hendrikx, V.L. Svetchnikov, R.J. Westerwaal, and B. Dam, J. Appl. Phys. 105 (2009) 043514.
[11] A. van Veen, H. Schut, J. de Vries, R.A. Hakvoort, and M.R. IJpma, AIP Conf. Proc. Vol. 218 (1990) 171.
[12] M.J. Puska and R.M. Nieminen, J. Phys. F: Met. Phys. 13 (1983) 333-346.
[13] J.M. Campillo Robles, E. Ogando, and F. Plazaola, J. Physics: Cond. Matter 19 (2007) 176222.
[14] P. Vermeulen, P.C.J. Graat, H.J. Wondergem, P.H.L. Notten, Int. J. Hydrogen Energy 33 (2008) 5646-5650.
[15] M. Clement, J.M.M. de Nijs, P. Balk, H. Schut, and A. van Veen, J. Appl. Phys. 79 (1996) 9029-9036.
[16] M.J. Puska, P. Lanki, and R.M. Nieminen, J. Phys.: Cond. Matter 1 (1989) 6081-6093.
[17] M.A. van Huis, A. van Veen, H. Schut, C.V. Falub, S.W.H. Eijt, P.E. Mijnarends, and J. Kuriplach, Phys. Rev B 65 (2002) 085416.
[18] G. Dlubek, S. Krause, H. Krause, K. Welpmann, and M. Peters, Scripta Metall. Mater. 27 (1992) 1049-1054.
[19] C.R. Luna, C.E. Macchi, A. Juan, and A. Somoza, Int. J. Hydrogen Energy 35 (2010) 12421-12427.
[20] S.E. Kulkova, O.N. Muryzhnikova, and K.A. Beketov, Int. J. Hydrogen Energy 21 (1996) 1041-1047.
[21] F. Plazaola, A.P. Seitsonen, and M.J. Puska, J. Phys.: Condens. Mat. 6 (1994) 8809-8827.
[22] F.M. Mulder, S. Singh, S. Bolhuis, and S.W.H. Eijt, J. Phys. Chem. C 116 (2012) 2001-2012.